Simulated Weld Pools Containing a Surface-Active Agent

Marangoni convection is reversed to go inward along the pool surface and downward toward the pool bottom, and deeper laser beam welds are produced when the agent is present

BY C. LIMMANEEVICHITR AND S. KOU

ABSTRACT. The theory that a surface-active agent can cause weld pool Marangoni convection to reverse itself – to go inward along the pool surface and downward toward the pool bottom and result in deeper weld penetration — was proposed by Heiple and Roper in 1982 and studied worldwide since then. To actually observe such a flow pattern, a simulated transparent weld pool of $NaNO_3$ (10 mm in diameter) was heated with a defocused CO_2 laser beam to induce Marangoni convection, and C_2H_5COOK was used as a surface-active agent to cause flow reversal. A laser light-cut technique was used to reveal convection in the pool. With pure $NaNO_3$, convection was outward along the free surface and downward along the pool wall. However, when C_2H_5COOK was present (*e.g.*, at 0.5 and 1 mole-%), convection slowed down. When more C_2H_5COOK was present (*e.g.*, at 1.5 and 2 mole-%), convection was reversed to go inward along the pool surface and downward along the pool axis. Since this is in the opposite direction of gravity-induced buoyancy convection, Marangoni convection clearly dominated in the pools. In stationary laser beam welding, $NaNO_3$ containing 1 mole-% C_2H_5COOK showed deeper weld pools and inward surface flow, while pure $NaNO_3$ showed shallower weld pools and outward surface flow. This is consistent with the reversal of Marangoni convection caused by C_2H_5COOK observed in the flow visualization.

C. LIMMANEEVICHITR and S. KOU are Graduate Student and Professor, respectively, in the Department of Materials Science and Engi-

Introduction

Marangoni convection, also called surface-tension-driven convection or thermocapillary convection, can have a dramatic effect on the penetration depth of the resultant weld. This was described in the well-known work by Heiple and Roper (Ref. 1).

Marangoni convection in a weld pool is illustrated in Fig. 1. The top view of the weld pool in Fig. 1A shows convection is outward along the pool surface. The front view of the pool in Fig. 1B shows the outward surface flow turns around at the pool edge, and the return flow below the pool surface is downward and inward.

The presence of the heat source near the center of the weld pool induces a negative temperature gradient along the pool surface, that is $T/s<0$, where T is temperature and s is the outward distance along the pool surface. In the absence of a surface-active agent, the surface tension γ decreases with increasing temperature, that is, $\gamma/T<0$ (Ref. 2).

As shown in Fig. 1B, a positive surface-tension gradient γ/s is present along the pool surface. Consequently, the liquid is pulled along the pool surface from the center (where temperature is high and the surface tension is low) to the edge (where temperature is low and the surface tension is high). Mathematically, $\gamma/s = T/s \times \gamma/T$. In other words, the surface-tension gradient γ/s (>0) is induced both by the temperature gradient along the pool surface T/s (<0) and the temperature dependence of the surface tension γ/T (<0).

The presence of a very small amount of a surface-active agent can make the weld pool much deeper (Ref. 1). The surface-active agent of a liquid, *e.g.*, S in liquid steel, is a material that can significantly reduce the surface tension of the liquid and even change its temperature dependence. It has been shown by thermodynamics (Ref. 3) and by experimental data (Refs. 4, 5) that in the presence of such an agent, the surface tension can, in fact, increase with increasing temperature, that is, $\partial\gamma/T>0$. This makes the surface-tension gradient along the pool surface negative, that is, $\partial\gamma/s<0$. As illustrated in Fig. 1C, the liquid is pulled along the pool surface from the edge (where temperature and the surface tension are both low) to the center (where temperature and the surface tension are both high). With the direction of flow reversed to favor convective heat transfer from the heat source to the pool bottom, a much deeper pool can be produced, as shown in Fig. 1D. General information about Marangoni convection in the weld pool is available elsewhere (Refs. 6, 7).

Marangoni convection cannot be studied in arc welding because of the interference by the electromagnetic force in the weld pool and by the aerodynamic drag force of the arc. To avoid this prob-

KEY WORDS

Marangoni Convection
Surface-Active Agent
Laser Beam Welding
Weld Pool
Gravity-Induced
Buoyancy Convection
Flow Visualization

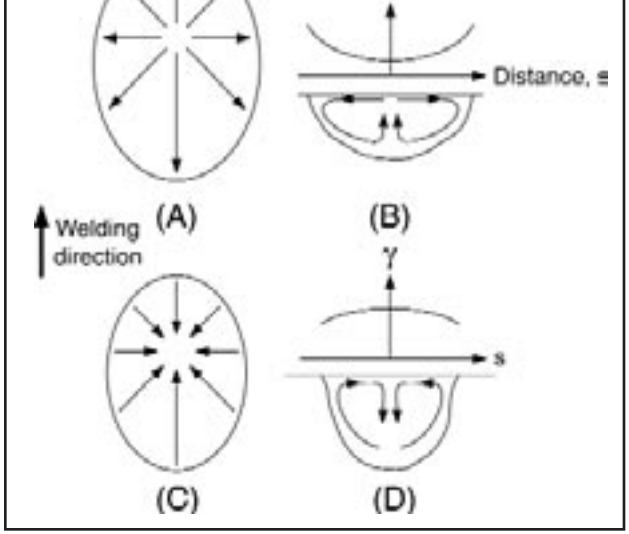

Fig. 1 — Marangoni convection in weld pools. A — Top view, convection outward; B — front view, outward convection turns and flow below surface is downward and inward; C — liquid pulled from pool edge to center; D — flow reversed to the pool bottom.

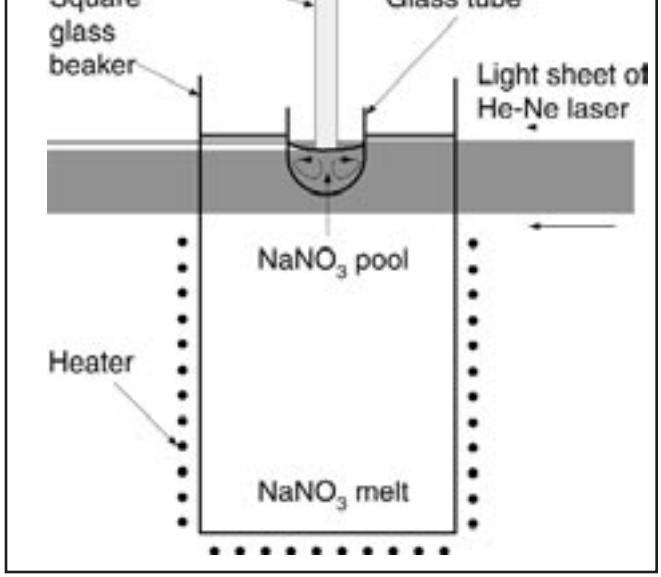

Fig. 2 — A transparent system for flow visualization of Marangoni convection in a simulated weld pool.

arc. As in arc welding, melting is through heating from the top surface (the so-called conduction mode), and no vapor hole is produced in the weld pool by the laser beam (the so-called keyholing mode). The Marangoni convection induced by such a defocused laser beam should be similar to that induced by a welding arc.

Flow visualization in a weld pool is limited to the pool surface because the molten metal is opaque. In fact, even at the pool surface such observation can still be difficult because of the brightness of the arc. Ishizaki, *et al*. (Ref. 8), observed Marangoni convection in a slice of molten paraffin heated by a soldering iron in contact with its top surface. Since paraffin is often a mixture of several organic compounds, its physical properties are not defined. Furthermore, it is not known if a surface-active agent is available for paraffin.

Recently, the authors have conducted physical simulation of weld-pool Marangoni convection by using a transparent pool of $NaNO_3$ and heating it with a defocused laser beam (Ref. 9). The physical properties of $NaNO_3$ are well documented, as will be shown later. The Marangoni number Ma for the simulated weld pool of $NaNO_3$ was close to those for steel and aluminum weld pools (Refs. 10–14). According to the similarity law of hydrodynamics, similarity in Marangoni convection between two fluid systems

In the present investigation, Marangoni convection in weld pools is simulated again using $NaNO_3$ but with C_2H_5COOK as a surface-active agent. The objectives are 1) to observe reversed Marangoni convection caused by a surface-active agent, and 2) to study the effect of the surface-active agent on the weld shape. Since the focus is on the observation of flow reversal and its effect on the weld shape, no attempt was made to measure the temperature and composition distributions along the pool surface and determine the Marangoni numbers.

Experimental Procedures

Materials

Sodium nitrate, $NaNO_3$, is a low-melting-point oxide and its physical properties are shown in Table 1 (Refs. 16–21). It has a transmission range of 0.35 to 3 μm and is, therefore, opaque to the CO_2 laser (10.6 μm) just like a weld pool is opaque to the heat source. Potassium propionate, C_2H_5COOK, decomposes at 330°C (Refs. 10, 16). The purity levels were above 99.99 and 99% for $NaNO_3$ and C_2H_5COOK, respectively.

Flow Visualization

The apparatus for flow visualization, shown in Fig. 2, is identical to the one used previously for flow visualization in

essentially hemispherical pool of $NaNO_3$ and a square Pyrex glass beaker (40 x 40 mm inside) holding a $NaNO_3$ melt.

A defocused CO_2 laser beam shone at the center of the pool surface to induce Marangoni convection. The characteristics of the CO_2 laser have been described (Ref. 9). The beam power was measured with a power meter having a 0.1-W resolution. The beam diameter was measured with a micrometer-mounted device developed recently (Ref. 9).

The $NaNO_3$ melt in the square beaker served to correct the optical distortion caused by the lens effect of the pool and to keep the pool from freezing and becoming opaque. The refractive index of $NaNO_3$ (1.46) is practically identical to that of Pyrex glass (1.47). A thermocouple was placed in the glass beaker near the bottom and hooked up to a temperature controller set at 330°C. In the absence of a CO_2 laser beam, this gave a temperature of 323.4°C at the bottom of the outer surface of the glass tube.

The amount of $NaNO_3$ in the glass tube was 630 mg. The tube was placed in the glass beaker to melt the $NaNO_3$ in the glass tube. A small amount of C_2H_5COOK, ranging from 2.5 to 10 mg, was added to the $NaNO_3$ pool at the pool temperature below 320°C. An electronic balance with 0.1-mg resolution was used for weighing. After the addition, the glass tube was removed from the beaker and shaken for two seconds before it was put

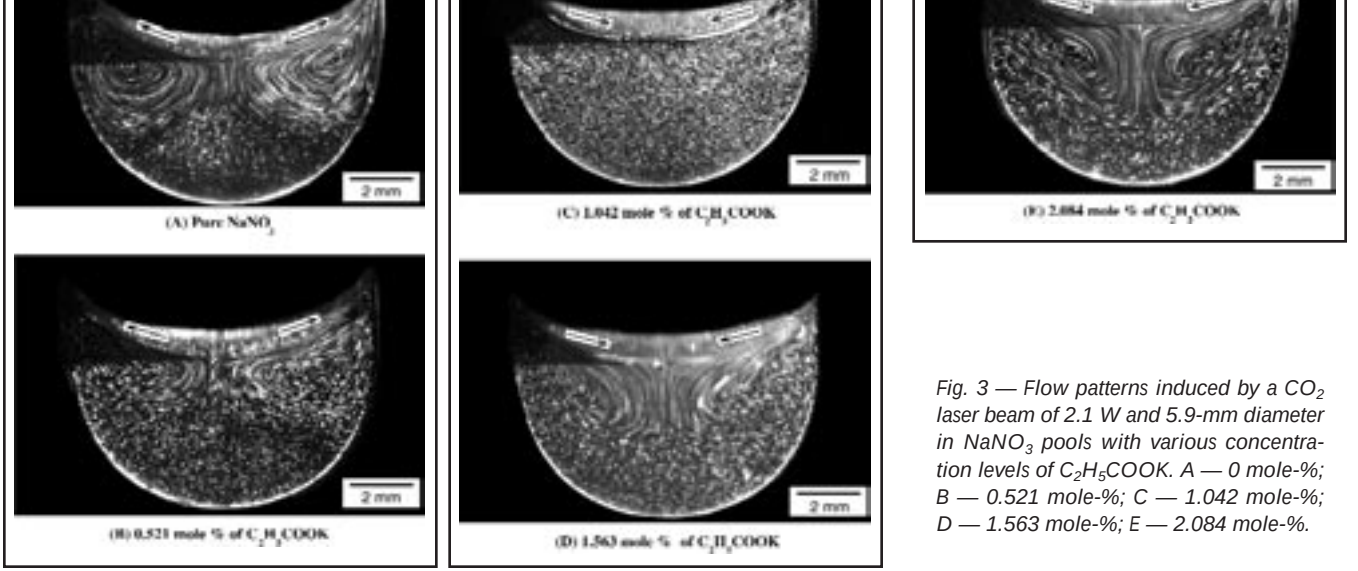

Fig. 3 — Flow patterns induced by a CO_2 laser beam of 2.1 W and 5.9-mm diameter in $NaNO_3$ pools with various concentration levels of C_2H_5COOK. A — 0 mole-%; B — 0.521 mole-%; C — 1.042 mole-%; D — 1.563 mole-%; E — 2.084 mole-%.

pool surface and flow visualization was started. All photographs were taken within 20 to 40 s.

A laser light-cut technique was used for flow visualization. The laser light sheet was produced with the help of a 20-mW He-Ne laser and optical lenses. It cut through the meridian plane of the pool to illuminate to the tracer particles in the melt and reveal the flow pattern. Aluminum particles 5 μm in diameter were used as a tracer. The density of aluminum (2.7 g cm^{-3}) is greater than that of the $NaNO_3$ melt (1.9 g cm^{-3}). From Stokes' law (Ref. 7), however, the settling velocity is much slower than Marangoni convection in view of the small particle diameter. In fact, aluminum particles are often used for flow visualization in water (Ref. 22), which is even lighter than $NaNO_3$. A certain amount of aluminum particles gradually settled to the pool bottom over extended periods of time. Photographs of the flow patterns were taken with Kodak Technical Pan films and an exposure time of 0.625 s. The reflex mirror of the camera was locked to reduce vibration.

Similar photographs were taken with a much shorter exposure time of 0.05 s with high-speed Kodak T-MAX P3200 films. The negatives were developed and scanned into the computer with a high-resolution scanner (maximum resolution 3200 dpi). The lengths of the velocity vectors were determined by using the x and y coordinates in the Info Palette displays in Adobe Photoshop 5.5 (Ref. 23). From the lengths of the flow lines and the

tors were interpolated using the inverse-distance interpolation function in Tecplot (Ref. 24) on a 27 x 28 grid that fits the free surface, wall and centerline of the pool.

Laser Beam Welding

Blocks of $NaNO_3$ were prepared for welding by melting and casting. The top and bottom surfaces were ground flat and cleaned before welding. The dimensions of the samples were 10 x 10 x 2 cm.

Stationary welds were made with a defocused CO_2 laser beam. The welding time was up to three minutes. The melt was then decanted from the pool instantaneously. Since the melt solidifies slowly, there was enough time for decanting.

The shape of the emptied pool was determined by using a digital x-y stage with a resolution of 0.01 mm and a fine-tip dial indicator with a resolution of 0.025 mm. The depth of the pool was measured every 0.25 mm along the diameter, in two directions perpendicular to each other.

Results and Discussion

Flow Pattern

Figure 3 shows the flow patterns induced by a CO_2 laser beam of 2.1 W power and 5.9 mm diameter. The melt wets the glass tube and forms a meniscus that makes the pool surface concave, though the pool surface can often be concave in conduction-mode laser

The arrows above the pool surface indicate the directions of flow along the pool surface. A dark shadow is present below the left-hand edge of the pool surface because this part of the pool surface reflects the laser light sheet coming from the right. The front half of the concave free surface faces the camera and acts as a mirror to show the illuminated meridian plane to the camera. This produces a bright image above the entire pool surface. The arrows are shown inside the range of this image.

Figure 3A shows the flow pattern in a pool of pure $NaNO_3$. Fluid flow is steady, axisymmetric and unicellular, somewhat similar to the shape of a doughnut. In the meridian plane of the pool, however, the flow pattern appears as a clockwise cell on the right and a counterclockwise cell on the left. In other words, the melt at the center of the pool surface flows outward along the pool surface, turns downward at the pool edge to fall along the pool wall, and then returns to the center of the pool surface. The flow lines are most closely spaced near the pool surface and become more widely separated below the pool surface and in the interior. This is consistent with the fact the surface flow is much faster than the return flow. There is little flow in the area near the bottom of the pool. The centers of the cells are close to the pool edge. These characteristics of Marangoni convection are confirmed by the videotape movie recorded during flow visualization (Ref. 27).

Figure 3B shows the flow pattern for a $NaNO_3$ pool containing 0.521 mole-% of

evident from the fact the flow lines are shorter than those in Fig. 3A.

As shown in Fig. 3C, when the C_2H_5COOK concentration is increased to 1.042 mole-% (50 mg), convection is reversed — the surface flow is now inward toward the center of the pool surface. Convection is weak, as indicated by the short flow lines. The flow pattern is not steady but changes slowly with time. However, the direction of convection remains unchanged, that is, always inward along the pool surface.

Figure 3D shows the case in which the C_2H_5COOK concentration is further increased to 1.563 mole-% (75 mg). As shown in Fig. 3D, the inward surface flow becomes faster. The downward flow along the pool axis penetrates deeper, about halfway to the pool bottom.

The case of the highest C_2H_5COOK concentration of 2.084 mole-% (100 mg) is shown in Fig. 3E. As compared to the previous case in Fig. 3D, convection is stronger, the liquid penetrates closer to the pool bottom and the flow lines are longer. This convection is in the opposite direction of gravity-induced buoyancy convection, and this indicates Marangoni convection dominates in the pool.

Higher C_2H_5COOK concentrations than 2.084 mole-% were also attempted, but there was a tendency for a film to form on the pool surface and for bubbles to form suddenly.

The flow patterns shown in Figs. 3C through 3E all change slowly with time. The flow cells move slowly without a clear frequency or amplitude. This is why some flow lines in Fig. 3E appear to cross each other. Within the 0.625-s exposure time, the flow pattern has changed slightly. The flow pattern in Fig. 3A for pure $NaNO_3$ is stable, as already mentioned. It is not suggested, however, that Marangoni convection with a strong outward surface flow is always stable. In fact, Marangoni convection in pure $NaNO_3$ becomes oscillatory when the laser power is increased beyond a certain point.

According to Table 1, C_2H_5COOK reduces the surface tension of $NaNO_3$ significantly, the concentration dependence of the surface tension being –22 dyne/(cm mole-%). Above 330°C, C_2H_5COOK decomposes as follows (Refs. 15, 21):

$$2C_2H_5COOK \rightarrow CH_3COOK + C_2H_5CHO\uparrow + C + KOH \qquad (1)$$

Melting point, T_m,°C	306.8
Decomposition temperature, T_d, °C	380
Autoignition point, T_a, °C	538
Heat of Fusion, ΔH, J/g	182
Temperature coefficient of surface tension, $\gamma\partial$ T, dyne/(cm °C)	–0.056
Surface tension, γ, dyne/cm	119.96 at T_m
Dynamic viscosity, μ, g/(cm s)	0.0302 at T_m
Density, ρ, g/cm^3	1.904 at T_m
Specific heat, C_p, J/(g °C)	1.71 at T_m
Thermal conductivity,k, W/(cm °C)	5.65 x 10^{-3} at T_m
Thermal expansion coefficient, β,°C^{-1}	6.6 x 10^{-4}
Thermal diffusivity, $\alpha = k/(\rho C_p)$, cm^2/s	1.74 x 10^{-3} at T_m
Prandtl number, $Pr = C_p\mu/k$	9.12 at T_m
Refractive index, n	1.46
Emissivity, ε	0.3
Transmission range, λ, cm	0.35 x 10^{-4} – 3 x 10^{-4}
Concentration dependence of surface tension for C_2H_5COOK, dyne/(cm mole-%)	–22
Concentration dependence of surface tension for CH_3COOK, dyne/(cm mole-%)	–4

boiling point 49°C), just escapes as a gas.

Unlike C_2H_5COOK, CH_3COOK does not reduce the surface tension of $NaNO_3$ much and can, therefore, be neglected for simplicity of discussion. The concentration dependence of the surface tension for CH_3COOK, –4 dyne/(cm mole-%), is less than one-fifth of that for C_2H_5COOK, –22 dyne/(cm mole-%) (Table 1). C and KOH are not known to have a significant effect on the surface tension of $NaNO_3$.

The way C_2H_5COOK can cause Marangoni convection in a laser-heated pool of $NaNO_3$ to be reversed is illustrated in Fig. 4. C_2H_5COOK in the pool decomposes upon heating by the laser beam. This makes the C_2H_5COOK concentration lower at the center of the pool surface and higher at the pool edge. Since C_2H_5COOK reduces the surface tension of $NaNO_3$ significantly, the surface tension can be higher at the center of the pool surface and lower at the pool edge. Consequently, Marangoni convection can be reversed to go inward along the pool surface and downward along the pool axis.

However, it should be cautioned that composition and

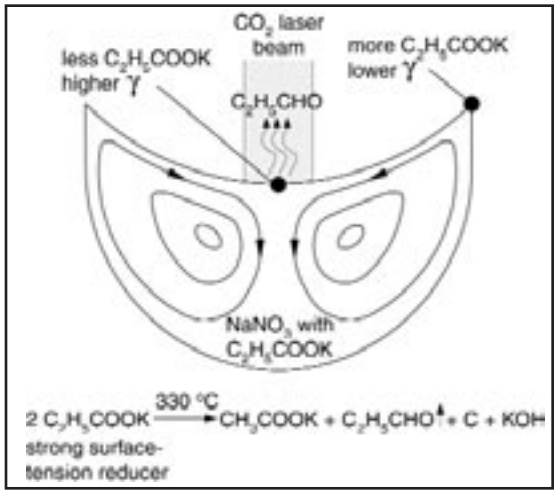

Fig. 4 — Reversed Marangoni convection in a $NaNO_3$ pool containing C_2H_5COOK,which decomposes upon heating by the laser beam.

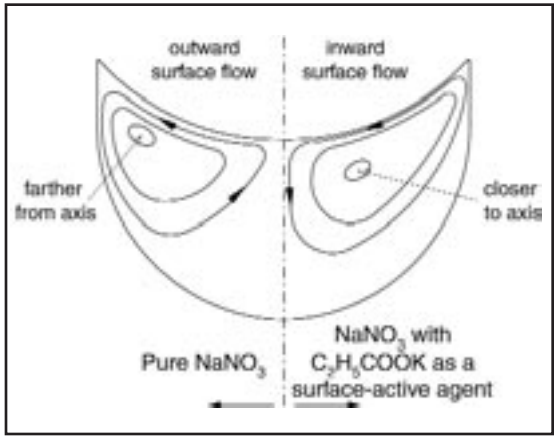

Fig. 5 — Effect of C_2H_5COOK on the flow pattern

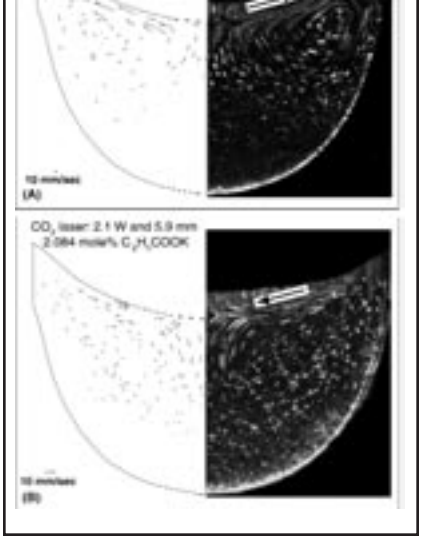

Fig. 6 — Velocity vectors measured in pools of the following: A — $NaNO_3$; B — $NaNO_3$ containing 2.084 mole-% C_2H_5COOK.

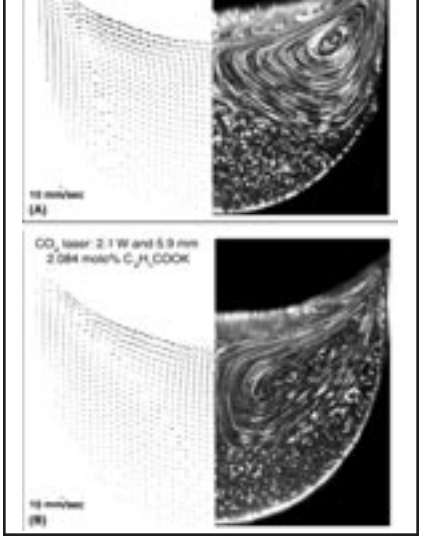

Fig. 7 — Velocity fields interpolated from measured velocity vectors. A — $NaNO_3$; B — $NaNO_3$ containing 2.084 mole-% C_2H_5COOK.

because $\partial\gamma/\partial T < 0$ (table 1). Consequently, the temperature gradients are in favor of a lower surface tension at the center of the pool surface and a higher surface tension at the pool edge, that is, an outward surface flow. This is just the opposite of the composition gradients along the pool surface. If the effect of composition gradients prevails over that of the temperature gradients, convection will be inward along the pool surface and vice versa.

Let s be the distance along the pool surface from the center of the pool surface, γ the surface tension, C the concentration of the surface-active agent, and T temperature. Since γ is a function of both C and T, the variation of the surface tension along the pool surface is as follows:

$$\frac{d\gamma}{ds} = \underbrace{\frac{\partial\gamma}{\partial T}}_{<0}\underbrace{\frac{dT}{ds}}_{<0} + \underbrace{\frac{\partial\gamma}{\partial C}}_{<0}\underbrace{\frac{dC}{ds}}_{<0} \qquad (2)$$

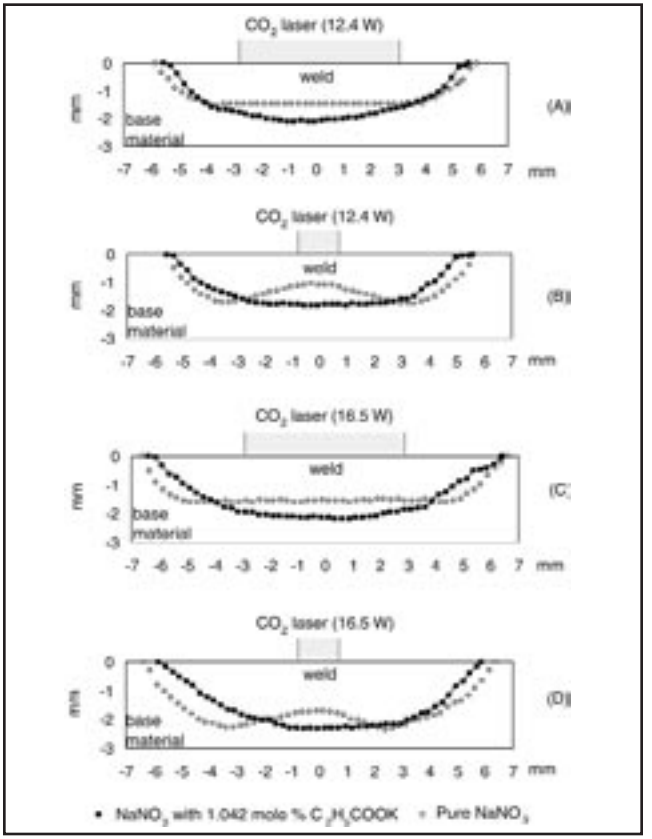

Fig. 8 — Shapes of stationary welds in solid $NaNO_3$ containing 1.042 mole-% C_2H_5COOK (squares) and pure $NaNO_3$ (open circles) produced by CO_2 laser beams. A — 12.4 W and 5.9 mm diameter; B —

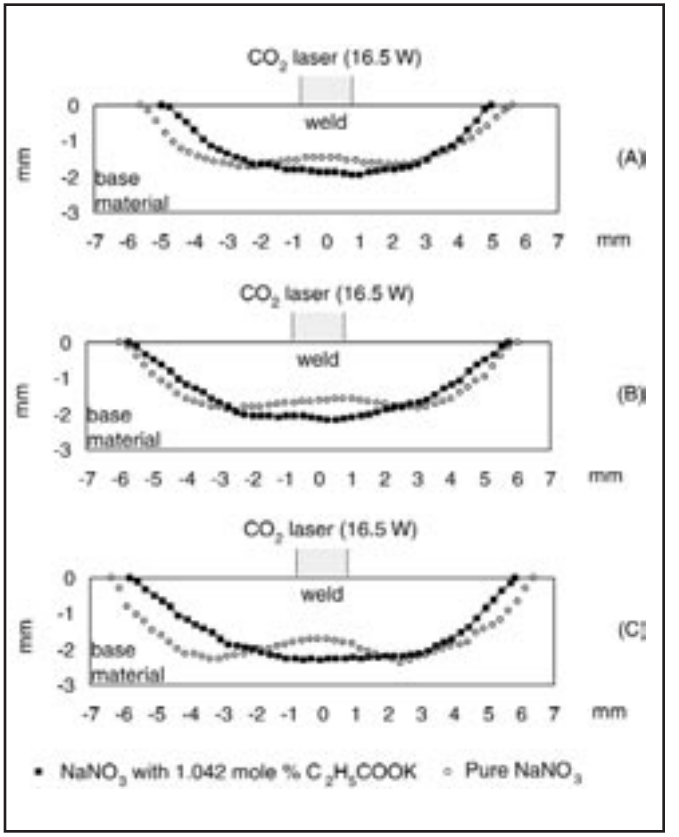

Fig. 9 — Shapes of stationary laser welds in solid $NaNO_3$ containing 1.042 mole-% C_2H_5COOK after at a welding time of: A — 1 min; B — 2 min; C — 3 min. Beam power: 16.5 W; beam diameter: 1.5 mm.

is, $\partial\gamma/\partial T < 0$ and $\partial\gamma/\partial C < 0$. When moving outward along the pool surface, temperature decreases but the C_2H_5COOK concentration increases, that is, $dT/ds < 0$ but $dC/ds > 0$. As such, the first term on the RHS of Equation 2 is positive but the second term is negative, and the sum of the two can either be positive or negative. If the surface tension varies along the pool surface more with temperature than with composition, the sum is positive and the surface flow is outward — Fig. 3A, B. On the other hand, if the surface tension varies along the pool surface more with composition than with temperature, the sum is negative and the surface flow is inward — Fig. 3C – E.

The effect of C_2H_5COOK is summarized in Fig. 5. When the levels of C_2H_5COOK concentration and heat source power are such that the surface tension decreases outward along the pool surface, Marangoni convection is reversed. Convection becomes inward along the pool surface and downward along the pool axis, and the centers of cells move away from near the pool edge toward the pool axis.

Velocity Fields

The right-hand side of Fig. 6 shows the short flow lines obtained by photographing with the short exposure time of 0.05 s. The left-hand side shows the velocity vectors measured from the flow lines. The flow lines are longer and have a greater tendency to overlap at the pool surface than in the interior, and their lengths are thus more difficult to measure.

The velocity vectors shown in Fig. 6A for pure $NaNO_3$ are outward near the pool surface and inward in the interior while those shown in Fig. 6B for $NaNO_3$ with 2.084 mole-% C_2H_5COOK are opposite in direction. On the average, the velocity vectors are longer in $NaNO_3$ than in $NaNO_3$ with 2.084 mole-% C_2H_5COOK. This is consistent with the observation of stronger convection in the former and weaker convection in the latter during flow visualization. The flow is weaker in the latter because composition and temperature gradients along the pool surface act in the opposite directions.

The velocity vectors in Fig. 6 are interpolated and shown in Fig. 7, along with the corresponding flow patterns photographed with the exposure time of 0.625 s. Unlike the velocity vectors in Fig. 6, these velocity fields cover the maximum velocity for $NaNO_3$ with 2.084 mole-% C_2H_5COOK is 10.7 mm/s, inward and pointing along the pool surface. It is also located at a radius of 2.76 mm along the free surface. In general, the velocities at the pool surface are not as accurate as those below it because of fewer available flow lines at the pool surface — Fig. 6.

Pool Shapes

Figure 8 shows stationary laser welds made in solid blocks of $NaNO_3$ and $NaNO_3$ with 1.04 mole-% C_2H_5COOK. The laser powers are 12.4 and 16.5 W, the beam diameters are 5.9 and 1.5 mm, and the welding time is 3 min. The solid squares represent the welds in $NaNO_3$ blocks containing 1.04 mole-% C_2H_5COOK that are made in the present study. The open circles indicate the welds in pure $NaNO_3$ blocks that were made in a previous study (Ref. 28). As shown in Fig. 8, the presence of C_2H_5COOK in $NaNO_3$ increases the weld depth at the pool axis and decreases the average weld width.

The laser powers of 12.4 and 16.5 W for welding are much higher than the laser power of 2.1 W for inducing Marangoni convection in the 10-mm pool. This is because in welding the laser beam has to be powerful enough to heat and melt the solid material to form a weld pool. As such, decomposition of C_2H_5COOK at the center of the pool surface and hence the composition gradients along the pool surface are expected to be more significant than those in the 10-mm-diameter pool. At the same time, however, temperature gradients along the pool surface also become more significant.

Since solid $NaNO_3$ is opaque, the flow pattern in the weld pool cannot be observed by the light-cut technique. However, the surface bubbles produced by the decomposition of C_2H_5COOK can still show the direction of the surface flow. They move inward along the weld pool surface before bursting near the center of the pool surface, and this indicates the surface flow is inward. As already shown by flow visualization, when the surface flow is inward, the flow, and hence convective heat transfer along the pool axis, are downward toward the pool bottom. This explains why the depth/width ratios in the welds containing 1.04 mole-% C_2H_5COOK are higher than those in the welds of pure $NaNO_3$. Therefore, flat. As the beam diameter is reduced from 5.9 to 1.5 mm, however, the power density, and hence the temperature at the center of the pool surface, increase significantly. The increased surface-tension gradients along the pool surface make the outward surface flow strong enough to turn downward at the pool edge and carry heat downward. Consequently, the pool is deeper near the pool edge than at the pool axis, that is, the pool bottom becomes convex. In the weld pools of $NaNO_3$ containing 1.04 mole-% C_2H_5COOK, however, the outward surface flow no longer exists, and the pool bottom is no longer convex.

As C_2H_5COOK decomposes with time, its concentration in the weld pool decreases. It is possible that beyond a certain point of time the pool depth actually begins to decrease because of little C_2H_5COOK left in the pool. In other words, strong outward surface flow takes over and the pool bottom starts to turn convex just like in a pure $NaNO_3$ pool. Figures 9A, B and C show the weld pool shapes in $NaNO_3$ containing 1.042 mole-% C_2H_5COOK after a welding time of 1, 2 and 3 min, respectively. As shown, the pool depth continues to increase within the 3 min period of time. This suggests that the 3 min welding time for the welds shown previously in Fig. 8 is appropriate.

Conclusions

Reversed Marangoni convection, caused by the presence of a surface-active agent to go inward along the pool surface and downward toward the pool bottom, can be observed in a simulated weld pool of $NaNO_3$ containing C_2H_5COOK as a surface-active agent and heated from above by a defocused CO_2 laser beam. Flow visualization can be achieved by using a laser light-cut technique to reveal convection in the pool. With pure $NaNO_3$, convection is outward along the free surface and downward along the pool wall. However, when C_2H_5COOK is added, convection slows down. With further addition of C_2H_5COOK, convection can be reversed to become inward along the pool surface and downward along the pool axis. Since this is in the opposite direction of gravity-induced buoyancy convection, Marangoni convection clearly dominates in the pool. In each pool, the laser light sheet intersects the doughnut-shaped flow cell twice and "two" counterrotating

deeper in $NaNO_3$ containing about 1 mole-% C_2H_5COOK than in pure $NaNO_3$. This is consistent with reversal of Marangoni convection by C_2H_5COOK observed in flow visualization. The downward flow along the pool axis carries heat from the laser beam to the pool bottom and makes it deeper.

Acknowledgments

This work was supported by NASA under Grant No. NAG8-1459. The authors thank Professor D. Schwabe for discussion on experiments.

References

1. Heiple, C. R., and Roper, J. R. 1982. Mechanism for minor element effect on GTA fusion zone geometry. *Welding Journal* 61(4): 97-s to 102-s.

2. Lida, T., and Guthrie, R. I. L. 1988. *The Physical Properties of Liquid Metals*. Oxford University Press, Oxford, England, p. 71, 92, 134, 183, 240.

3. Sahoo, P., DebRoy, T., and McNallan, M. J. 1988. Surface tension of binary metal — surface active solute systems under conditions relevant to welding metallurgy. *Metallurgical Transactions* 19B(3): 483–491.

4. Mills, K. C., Keene, B. J., Brooks, R. F., and Olusanya, A. 1984. Surface tension of 304 and 316 type stainless steels and their effect on weld penetration. Report of the National Physical Laboratory, Teddinton, Middlesex, UK.

5. Sundell, R. E., Correa, S. M., Harris, L. P., Solomon, H. D., Wojcik, L. A., Savage, W. F., Walsh, D. W., and Lo, G. –D. 1986. Minor

York, N.Y., John Wiley and Sons. pp. 91–103.

7. Kou, S. 1996. *Transport Phenomena and Materials Processing*. John Wiley and Sons, N.Y., pp. 44–48, 499–515.

8. Ishizaki, K., Araki, N., and Murai, H. 1965. Penetration in arc welding and convection in molten metal. *Journal of Japan Welding Society* 34(2): 146–153. (in Japanese)

9. Limmaneevichitr, C., and Kou, S. 1999. Visualization of Marangoni convection in simulated weld pools. *Welding Journal* 79(5): 126-s to 135-s.

10. Oreper, G. M., and Szekely, J. 1984. Heat- and fluid-flow phenomena in weld pools. *Journal of Fluid Mechanics* 147: 53–79.

11. Pitscheneder, W., Ebner, R., DebRoy, T., and Mundra, K. 1996. Weld pool geometry during high power conduction mode carbon dioxide laser welding. *Trends in Welding Research*, eds. Smart, H. B., Johnson, J. A., and David, S. A. ASM International, Materials Park, Ohio.

12. Kim, W. H., Fan, H. G., and Na, S. J. 1997. Effect of various driving forces on heat and mass transfer in arc welding. *Numerical Heat Transfer*, Part A 32: 633–652.

13. Kou, S., and Sun, D. K. 1985. Fluid flow and weld penetration in stationary arc welds. *Metallurgical Transactions* A, 16A: 203–213.

14. Tsai, M. C., and Kou, S. 1989. Marangoni convection in weld pools with a free surface. *Internal Journal for Numerical Methods in Fluids* 9: 1503–1516.

15. Schwabe, D., Scharmann, A. Preisser, F., and Oeder, R. 1978. Experiments on surface tension driven flow in floating zone melting. *Journal of Crystal Growth* 43: 305–312.

16. White, L. R., and Davis, H. T. 1967.

Chemistry, Reference Data 1(3): 583–704.

18. Preisser, F., Schwabe, D., and Scharmann, A. 1983. Steady and oscillatory thermocapillary convection in liquid columns with free cylindrical surface. *Journal of Fluid Mechanics* 126: 545–567.

19. Atomergic Chemetals Corporation. 1993. Datasheet. Farmingdale, N.Y.

20. Alfa AESAR. 1999. Material safety data sheet for $NaNO_3$. Ward Hill, Mass.

21. Smechenko, V. K., and Shikobalova, L. P. 1947. Surface tension and crystallization: surface tension of molten salt solutions. *Zh. Fiz. Khim.* 21:613– 622. (in Russian)

22. Rouse, H. 1978. *Elementary Mechanics of Fluids*. Dover Publications, New York, N.Y., p. 39.

23. Adobe Systems Inc. 1999. Adobe Photoshop Version 5.5, San Jose, Calif.

24. Amtec Engineering, Inc. 1998. Tecplot Version 7.5, Bellevue, Wash.

25. Duley, W. W. 1999. *Laser Welding*. New York, N.Y.: John Wiley and Sons. p. 76.

26. Mazumder, J., and Voekel, D. 1992. *Laser Advanced Materials Processing — Science and Applications*. Eds. Matsunawa, A. and Katayama, S. High Temperature Society of Japan. Osaka, Japan. Vol. 1, pp. 373–380.

27. Limmaneevichitr, C., and Kou, S. 2000. Flow visualization of Marangoni convection in a simulated weld pool (a videotape movie). Presented at American Welding Society 81st Annual Convention, April 25–28, 2000, Chicago, Ill.

28. Limmaneevichitr, C., and Kou, S. 1999. Experiments to simulate effect of Marangoni convection on weld pool shape. *Welding Journal* 79(8): 231-s to 237-s.